

Multi-modal thermoacoustic instability suppression via locally resonant and Bragg bandgaps

Yang Liu, Li Cheng and Jingtao Du

Citation: [The Journal of the Acoustical Society of America](#) **152**, 3471 (2022); doi: 10.1121/10.0016554

View online: <https://doi.org/10.1121/10.0016554>

View Table of Contents: <https://asa.scitation.org/toc/jas/152/6>

Published by the [Acoustical Society of America](#)


JASA
THE JOURNAL OF THE
ACOUSTICAL SOCIETY OF AMERICA

**Special Issue: Fish Bioacoustics:
Hearing and Sound Communication**

CALL FOR PAPERS



Multi-modal thermoacoustic instability suppression via locally resonant and Bragg bandgaps

Yang Liu,¹ Li Cheng,²  and Jingtao Du^{1,a)}

¹College of Power and Energy Engineering, Harbin Engineering University, Harbin 150001, China

²Department of Mechanical Engineering, The Hong Kong Polytechnic University, Hung Hom 999077, Hong Kong

ABSTRACT:

Thermoacoustic instability is a common occurrence in combustors, yielding self-sustained oscillations and causing potential risk, such as severe structural damage. In this paper, modal instability suppression inside a duct is studied using periodically arranged membranes within the framework of a linear heat release n - τ model embedded into a fully coupled energy-based model. The periodic arrangement of the membranes along the duct side-wall enables locally resonant and Bragg scattering bandgaps, shown to be conducive for the stabilization of unstable thermoacoustic modes. Eigen-modes are classified into different groups, which call for specific control actions in relation with the bandgap frequencies. While multi-modal instability control of low-order modes can be achieved through the tuning of the resonant bandgaps, the densely packed modal cluster, regrouping modes featuring similar mode shapes, requires proper adjustment of the flame position for avoiding modal instability. Compared with the Bragg bandgaps, locally resonant bandgaps, which should be formed near the unstable modes even without stringent periodicity, are shown to play a decisive role in the control process. Meanwhile, strict periodicity is not necessary for the proposed control strategy, showing the practicability of the proposed control strategy. The study shows a promising route to achieve simultaneous suppression of multi-modal instability.

© 2022 Acoustical Society of America. <https://doi.org/10.1121/10.0016554>

(Received 6 August 2022; revised 26 November 2022; accepted 28 November 2022; published online 13 December 2022)

[Editor: Marcel C. Remillieux]

Pages: 3471–3482

I. INTRODUCTION

Low-emission and high-power density combustors represent the future development trend in modern gas turbines. With the demand for increasing efficiency, thermoacoustic instability (TAI) is a common occurrence and becomes a major concern.^{1–3} TAI occurs as the result of strong interaction between the acoustic field and the heat source/flame in a combustor, forming a positive energy feedback in the interaction loop. The phenomenon leads to unacceptable vibration/noise in power and energy systems, which might also generate the structural fatigue to jeopardize their operation and safety. It was demonstrated that TAI is triggered when the unsteady rate of the heat input is in phase with the acoustic pressure perturbation.^{4,5} In that sense, acoustic modal characteristics exert vital influence on TAI.^{6,7} In addition to acoustic modes, which mainly depend on the system geometry, intrinsic modes were also shown to exist by recent research.^{8–10} Studies show that the heat source or flame can give rise to a completely new family of system modes due to the local feedback loop formed in the coupled system.

Based on the existing understanding of the physical mechanism behind TAI, intensive efforts were devoted to suppressing the acoustic pressure oscillations and preventing the onset of such an instability process. Typical methods can be loosely grouped into passive and active control methods.

Among existing methods, improving burning conditions was extensively exploited, such as changing the fuel injection flow rates or using hydrogen fuel.^{11,12} Such methods, however, usually require a complex fuel control system. As an alternative, acoustic modulation strategies have attracted persistent attention in the TAI control community.

Active control of the acoustic oscillations can directly modulate the sound pressure field. Upon monitoring dynamics in the combustor, the measured signal is fed back to a control system for altering the thermoacoustic interaction. As a typical example, Heckl¹³ studied the active control of thermoacoustic oscillation in a Rijke tube. A physical and systematic model-based design of an active controller was reported by Hathout *et al.*,¹⁴ leading to a significantly faster settling time of the pressure oscillations. The concept of using feedback control to alter the interaction between the acoustic waves and unsteady heat release was introduced by Dowling and Morgans.¹⁵ For achieving enhanced efficiency and capability, a specific feedback control using a time-delayed integral algorithm was proposed by Olgac and Zalluhoglu.¹⁶ In addition, high-voltage microsecond pulsed plasma was also used as actuators to attenuate the thermoacoustic pressure waves in a Rijke tube.¹⁷ Despite its appealing adaptive feature, active control usually involves complex electronics and high cost alongside concerns over requirements regarding actuation authority, bandwidth, and durability/robustness. Therefore, passive control still remains an important alternative for TAI suppression.

^{a)}Electronic mail: dujingtao@hrbeu.edu.cn

Passive approaches are exemplified by measures such as redesign of combustion chambers (duct dimensions and burner location) and the installation of additional control devices such as baffles, resonators, and acoustic liners.^{18,19} Among these measures, the Helmholtz resonator (HR) is a simple and effective device for the suppression of thermoacoustic oscillation.²⁰ Past efforts include the design of the cavity size and aperture length/width and the use of multiple HRs in various combustion systems^{21–23} such as in a complex sound environment like flow medium.²⁴ In addition to the HRs, perforated liners have also attracted immense attention.^{25–27} Compared with HRs, perforated liners in a flow duct allow for a compact structural design and a significant damping enhancement at the same time. In addition, attempts were made through embedding the elastic membranes on a duct sidewall, whose configuration was determined through sophisticated numerical analyses and optimizations.²⁸ The underlying control mechanism underpinning the modal instability was revealed in the context of locally resonant flexible membranes.⁷ Studies show two different physical processes associated with acoustic and intrinsic modes, respectively. Despite their demonstrated success, passive methods are usually effective over a narrow frequency range or for specific targeted modes, thus, showing limited control capability, especially in complex combustion operating conditions. Therefore, a comprehensive strategy for multi-mode and broadband TAI control is lacking. This motivates the present work.

Compared with the traditional passive control means mentioned above, phononic crystals (PCs) have aroused increasing interest in the scientific community. When sound waves propagate in a periodic elastic medium, bandgaps can be generated, within which acoustic wave propagation is forbidden.^{29,30} These bandgaps are referred to as Bragg-reflection-based bandgaps (BBGs). Meanwhile, locally resonant structures can also generate a resonant bandgap (RBG) at sub-wavelength scale.³¹ The appealing physical properties of the periodic structures have been explored for various acoustic applications, including noise mitigation in ducts. A typical example is the study of periodically arranged HRs in a piping/duct system to obtain the low frequency bandgaps.^{32,33} In addition, side-branch tubes,³⁴ micro-perforated panels,³⁵ and flexible membranes^{36,37} have also been investigated to explore the benefits of bandgap features. Periodic structures allow for tailoring and manipulating acoustic wave propagation, which holds potential promise for modal instability control in thermoacoustic systems. However, studies using acoustic bandgaps for modal instability control, as well as the understanding of the physical mechanisms behind, still remain unclear and largely unexploited. This forms another motivation behind the present work.

This paper addresses the above challenges. More specifically, periodic membrane-cells are flush-mounted inside a heat duct to control its modal instability in the framework of a linear n - τ flame model. Numerical analyses are conducted based on a proposed energy-based semi-analytical model, in which pressure continuity is used for the description of

sound propagation in each membrane-cell unit. Numerical studies demonstrate how the modal instability can be altered by the deployment of the membranes depending on their respective modal nature. In particular, the influences of RBGs and BBGs on the modal TAI control are systematically investigated. Different from the traditional control devices, the bandgap features induced by the membrane tension and lattice are shown to be conducive to multi-modal instability control.

The remainder of this paper is organized as follows. The theoretical formulation of the problem under investigation is first presented. In Sec. III, the BBG and RBG properties are examined in the absence of flame. This is then followed by systematic studies on the modal instability control via periodic membranes, including the possibilities of customizing bandgap positions through adjusting system parameters and their impact on the global TAI control. Finally, conclusions are drawn.

II. MODEL DESCRIPTION

Consider the thermoacoustic system illustrated in Fig. 1. The system consists of a duct and several flexible structures (tensioned membranes by default), which are flush-mounted and periodically arranged along the duct walls. The first membrane position is determined by the two end points, x_1 and x_2 , and the distribution distance between two nearby membranes is denoted by D , also called the lattice length. The left end points of each membrane are marked as X_1, X_2, \dots, X_s . The duct (length L , height h) has two ends with the reflection coefficients denoted by R_0 and R_L , respectively. A compact flame is located at $x = x_q$, with a heat release rate $q'(x, t) = Q'(t)\delta(x - x_q)$, where $Q'(t) = Qe^{-i\omega t}$ and δ denotes the Dirac δ -function.

While the plane wave propagation can be considered in the rigid segments of the duct below its cut-on frequency, higher-order duct modes need to be considered for the flexible portions containing membranes, thus, resulting in the mutual interaction between the duct and flexible membranes. To tackle the problem, an energy-based approach is adopted to capture such vibroacoustic coupling behavior. The transverse vibrating displacement of the s th flexible membrane with fixed boundaries can be expanded as

$$w_s(x) = \sum_{q=1}^M a_s^q \sin(q\pi x_s/l) = \Psi_s(x_s) \mathbf{A}_s, \quad (1)$$

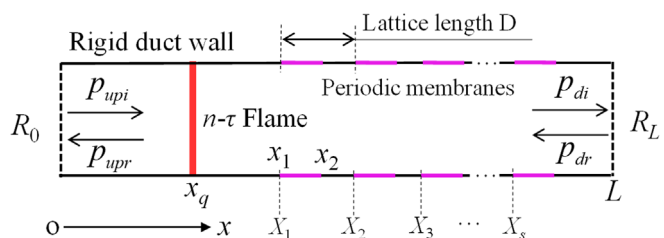


FIG. 1. (Color online) Schematic diagram of a thermoacoustic system with periodic membranes, flush-mounted in the duct sidewalls.

in which $x_s = x - x_1 - (s - 1)D$; M is the truncation term number of Fourier series, and l is the membrane length; Ψ denotes the mode shape vector. The *Lagrangian* of the s th membrane writes

$$L_s = U_s - T_s + W_s, \tag{2}$$

in which U_s and T_s denote the total potential and kinetic energies, respectively; W_s represents the work done by the sound pressure inside the duct over the upper surface of flexible membrane, namely,

$$U_s = \frac{1}{2}F \int_0^l \left[\frac{\partial w_s(x_s)}{\partial x_s} \right]^2 dx_s, \tag{3a}$$

$$T_s = \frac{1}{2}\omega^2 \rho_m \int_0^l w_s^2(x_s) dx_s, \tag{3b}$$

$$W_s = \int_0^l \left(p_s^{rad} + p_s^{ui} + p_{s+1}^{dr} \right) w dx_s, \tag{4}$$

where F and ρ_m are the tension force applied to the membrane and its mass density, respectively. p_s^{rad} is the sound pressure radiated by the s th membrane. p_s^{ui} is the upstream incident sound pressure and p_{s+1}^{dr} the downstream reflective sound pressure from the $(s + 1)$ th cell. The incident and reflected waves for the s th cell can be seen as the planar waves when the excitation frequency is much lower than the cut-on frequency of the duct. It follows

$$p_s^{ui} = C_s^{ui} e^{-ik\{x_s+x_1+sD-D\}}, \tag{5a}$$

$$p_{s+1}^{dr} = C_{s+1}^{dr} e^{ik(x_s+x_1+sD-D)}, \tag{5b}$$

in which C_s^{ui} and C_{s+1}^{dr} are the unknown sound pressure coefficients; $k = \omega/c$ is the acoustic wave number; ω is angular frequency; and c is the sound speed. The radiated sound pressure from the s th membrane can be estimated by³⁷

$$p_s^{rad}(x, y) = \frac{\rho}{2h} \sum_{m=0}^{\infty} \frac{\omega}{k_m} \psi_m(y) \int_0^l \psi_m(y')|_{y'=0} i\omega w_s \times G(x_s, x'_s) dx'_s, \tag{6}$$

in which $\psi_m(y)$ is the acoustic mode shape function of the duct; $G(x_s, x'_s)$ and k_m are Green's function and modal wave-number, respectively; and ρ represents the air density.

The Green's function writes

$$G = H(x - x')e^{-ik_m(x-x')} + H(x' - x)e^{+ik_m(x-x')}, \tag{7a}$$

$$k_m = \frac{\omega}{ic} \sqrt{(m\pi/k_0h)^2 - 1}, \tag{7b}$$

where H is the Heaviside function. Zero-order plane wave corresponds to $m = 0$, while higher-order modes correspond to $m > 1$.

Combining Eqs. (1)–(4) and using Lagrange's equations $(d/dt)(\partial L/\partial \dot{a}_q(t)) - (\partial L/\partial a_q(t)) = 0$ under harmonic

regime for the modal amplitude coefficients a_q yield a set of linear equations, casted into the following matrix form:

$$(\mathbf{K}_s - \omega^2 \mathbf{M}_s + i\omega \mathbf{G}_s) \mathbf{A}_s = \mathbf{P}_s^{ui} + \mathbf{P}_{s+1}^{dr}. \tag{8}$$

The unknown modal amplitude vector can then be determined as

$$\begin{aligned} \mathbf{A}_s &= (\mathbf{K} - \omega^2 \mathbf{M} + i\omega \mathbf{G})^{-1} (\mathbf{P}_s^{ui} + \mathbf{P}_{s+1}^{dr}) \\ &= \mathbf{\Pi} (\mathbf{P}_s^{ui} + \mathbf{P}_{s+1}^{dr}), \end{aligned} \tag{9}$$

in which \mathbf{K}_s and \mathbf{M}_s are the stiffness and mass matrices of the flexible membrane *in vacuo*, respectively; \mathbf{G}_s is the coupling matrix characterizing the membrane-duct interaction; and vectors \mathbf{P}_s^{ui} and \mathbf{P}_{s+1}^{dr} denote the work done by the sound pressure p_s^{ui} and p_{s+1}^{dr} , which can be expressed as

$$\begin{aligned} \mathbf{P}_s^{ui} &= C_s^{ui} e^{-ik(x_1+sD-D)} \int_0^l \Psi_s(x_s) e^{-ikx_s} dx_s \\ &= C_s^{ui} e^{-ik(x_1+sD-D)} \chi_s^{ui}, \end{aligned} \tag{10}$$

$$\begin{aligned} \mathbf{P}_{s+1}^{dr} &= C_{s+1}^{dr} e^{ik(x_1+sD-D)} \int_0^l \Psi_s e^{ikx_s} e^{-ikD} dx_s \\ &= C_{s+1}^{dr} e^{ik(x_1+sD-D)} \chi_{s+1}^{dr}. \end{aligned} \tag{11}$$

Based on the continuity of the sound pressure at the cross-sections X_s and X_{s+1} of the s th cell, one has

$$C_{s+1}^{ui} e^{-ik(x_1+sD)} = C_s^{ui} e^{-ik(x_1+sD)} + p_s^{rad+}, \tag{12}$$

$$C_s^{dr} e^{ik(x_1+sD-D)} = C_{s+1}^{dr} e^{ik(x_1+sD-D)} + p_s^{rad-}, \tag{13}$$

in which p_{rad}^+ and p_{rad}^- are the radiated sound pressure by the membrane in x -positive and $-$ negative directions, respectively, which can be simplified from Eq. (6) as

$$\begin{aligned} P_{rad}^+ &= e^{-ikD} \frac{\rho c}{2h} \int_0^l i\omega w(x'_s) e^{ikx'_s} dx'_s \\ &= e^{-ikD} \mathbf{P}_s^+ \mathbf{\Pi} (\mathbf{P}_s^{ui} + \mathbf{P}_{s+1}^{dr}), \end{aligned} \tag{14}$$

$$P_{rad}^- = \frac{\rho c}{2h} \int_0^l i\omega w(x'_s) e^{-ikx'_s} dx'_s = \mathbf{P}_s^- \mathbf{\Pi} (\mathbf{P}_s^{ui} + \mathbf{P}_{s+1}^{dr}), \tag{15}$$

where

$$\mathbf{P}_s^+ = \frac{\rho c}{2h} \int_0^l i\omega \Psi_s e^{ikx'_s} dx'_s, \tag{16a}$$

$$\mathbf{P}_s^- = \frac{\rho c}{2h} \int_0^l i\omega \Psi_s e^{-ikx'_s} dx'_s. \tag{16b}$$

Substituting Eqs. (14)–(16) into Eqs. (12) and (13) gives

$$C_s^{ui} \left(e^{-ik(x_1+sD)} + e^{-ik(x_1+sD)} \mathbf{P}_s^+ \mathbf{\Pi} \chi_s^{ui} \right) - C_{s+1}^{ui} e^{-ik(x_1+sD)} + C_{s+1}^{dr} e^{ik(x_1+sD-2D)} \mathbf{P}_s^+ \mathbf{\Pi} \chi_{s+1}^{dr} = 0, \quad (17)$$

$$C_s^{ui} e^{-ik(x_1+sD-D)} \mathbf{P}_s^- \mathbf{\Pi} \chi_s^{ui} - C_s^{dr} e^{ik(x_1+sD-D)} + C_{s+1}^{dr} \left(e^{ik(x_1+sD-D)} + e^{ik(x_1+sD-D)} \mathbf{P}_s^- \mathbf{\Pi} \chi_{s+1}^{dr} \right) = 0. \quad (18)$$

Based on the equation $X_s = x_1 + sD - D$, the above equations can then be simplified as

$$C_s^{ui} \left(e^{-ikX_s} + e^{-ikX_s} \mathbf{P}_s^+ \mathbf{\Pi} \chi_s^{ui} \right) - C_{s+1}^{ui} e^{-ikX_s} + C_{s+1}^{dr} e^{ikX_s} \mathbf{P}_s^+ \mathbf{\Pi} \chi_{s+1}^{dr} = 0, \quad (19)$$

$$C_s^{ui} e^{-ikX_s} \mathbf{P}_s^- \mathbf{\Pi} \chi_s^{ui} - C_s^{dr} e^{ikX_s} + C_{s+1}^{dr} \left(e^{ikX_s} + e^{ikX_s} \mathbf{P}_s^- \mathbf{\Pi} \chi_{s+1}^{dr} \right) = 0. \quad (20)$$

For the periodic membranes, a series of linear equations can be obtained from Eqs. (19) and (20), assembled as

$$\begin{bmatrix} e^{-ikX_1} (1 + \mathbf{P}_1^+ \mathbf{\Pi} \chi_1^{ui}) & 0 & -e^{-ikX_1} & e^{ikX_1} \mathbf{P}_1^+ \mathbf{\Pi} \chi_2^{dr} \\ & e^{-ikX_s} (1 + \mathbf{P}_s^+ \mathbf{\Pi} \chi_s^{ui}) & \dots & \dots \\ & e^{-ikX_s} \mathbf{P}_s^- \mathbf{\Pi} \chi_s^{ui} & -e^{ikX_s} & e^{ikX_s} \mathbf{P}_s^+ \mathbf{\Pi} \chi_{s+1}^{dr} \\ & & -e^{ikX_s} & e^{ikX_s} (1 + \mathbf{P}_s^- \mathbf{\Pi} \chi_{s+1}^{dr}) \\ & & \dots & \dots \\ 0 & e^{-ikX_{s-1}} \mathbf{P}_{s-1}^- \mathbf{\Pi} \chi_{s-1}^{ui} & -e^{ikX_{s-1}} & 0 \\ & & & e^{ikX_s} (1 + \mathbf{P}_{s-1}^- \mathbf{\Pi} \chi_s^{dr}) \end{bmatrix} \times \begin{bmatrix} C_1^{ui} \\ \dots \\ C_s^{ui} \\ C_s^{dr} \\ C_{s+1}^{ui} \\ C_{s+1}^{dr} \\ \dots \\ C_s^{dr} \end{bmatrix} = [\mathbf{0}]. \quad (21)$$

When ignoring the flame and combining the boundary conditions, one has

$$\frac{p_0^{ui}(0)}{p_L^{dr}(0)} = R_0 = \frac{C_1^{ui}}{C_1^{dr}}, \quad (22a)$$

$$\frac{p_L^{ui}(L)}{p_L^{dr}(L)} = R_L = \frac{C_s^{ui} e^{-ikL}}{C_s^{dr} e^{ikL}}. \quad (22b)$$

Based on the boundary conditions and coefficient matrix Eq. (22), dynamic characteristics of the duct coupled with periodic membranes can be investigated in the absence of flame. When considering a flame located at x_q as presented in Fig. 1, the sound pressure of upstream x_q^- and downstream x_q^+ can be expressed as

$$\begin{aligned} p_{x_q^-}^{ui} &= C_{x_q^-}^{ui} e^{-ikx_q}, & p_{x_q^-}^{dr} &= C_{x_q^-}^{dr} e^{ikx_q}, \\ p_{x_q^+}^{ui} &= C_{x_q^+}^{ui} e^{-ikx_q}, & p_{x_q^+}^{dr} &= C_{x_q^+}^{dr} e^{-ikx_q}. \end{aligned} \quad (23)$$

Using the sound pressure and mass conservation principle,¹⁰ one has

$$p_{x_q^-}^{ui} + p_{x_q^-}^{dr} = p_{x_q^+}^{ui} + p_{x_q^+}^{dr}, \quad (24)$$

$$v_{x_q^-}^{ui} + v_{x_q^-}^{dr} - (v_{x_q^+}^{ui} + v_{x_q^+}^{dr}) = -\frac{\gamma - 1}{\rho c^2} Q, \quad (25)$$

where v is the particle velocity. The right-hand-side part of Eq. (25) represents the velocity fluctuation generated by the unsteady rate of the flame heat release. In this work, a linear n - τ flame model is adopted,⁷ with the coefficient of heat release rate written as

$$Q = \frac{\rho c^2}{\gamma - 1} n e^{i\omega\tau} (v_{x_q^-}^{ui} + v_{x_q^-}^{dr}), \quad (26)$$

in which n and τ correspond to the flame interaction index and time-lag, respectively; γ denotes the specific heat ratio; and the term $n e^{i\omega\tau}$ represents the flame transfer function (FTF). Combining Eqs. (23)–(26) yields the following two linear equations:

$$C_{x_q^-}^{ui} e^{-ikx_q} + C_{x_q^-}^{dr} e^{ikx_q} = C_{x_q^+}^{ui} e^{-ikx_q} + C_{x_q^+}^{dr} e^{ikx_q}, \quad (27)$$

$$\begin{aligned} C_{x_q^-}^{ui} (e^{-ikx_q} + n e^{i\omega\tau} e^{-ikx_q}) + C_{x_q^-}^{dr} (-e^{ikx_q} - n e^{i\omega\tau} e^{ikx_q}) \\ = C_{x_q^+}^{ui} e^{-ikx_q} - C_{x_q^+}^{dr} e^{ikx_q}. \end{aligned} \quad (28)$$

Combining Eqs. (21), (22), (27), and (28) yields a series of homogeneous equations in terms of the unknown sound

pressure amplitudes C^{ui} and C^{dr} . The coefficient matrix should be arranged based on the position of the flame and that of the membranes. To obtain the nontrivial solutions of the eigen-problem, cast into the aforementioned linear equations, the determinant of the coefficient matrix needs to be zero. Then the eigenroots ω of the thermoacoustic coupling system can be obtained. Due to the existence of the heat source, these frequencies are generally complex, namely $\omega = \omega_{\text{real}} + i\omega_{\text{imag}}$, in which the real part ω_{real} is the natural frequency of the thermoacoustic coupling system, and the imaginary ω_{imag} is the growth rate (GR) of the corresponding mode, which characterizes its stability nature. When ω_{imag} is negative, the heat disturbance disappears within a short time, signaling a stable status. However, if ω_{imag} is positive, the system oscillation will grow exponentially with time and eventually lead to system instability. A numerical procedure as presented in Ref. 7 is used in this work to obtain the eigen-solutions of the above system, and the modal behavior of the thermoacoustic system is illustrated by the contour plots in the complex frequency plane.

In the current model, the backside of each membrane is the ambient atmosphere without cavity. Having said that, the consideration of a backing cavity in the study does not pose any technical difficulties, which is what we did before on other occasions. Our modeling framework is built upon sub-system Lagrangian, which allows very easy inclusion of additional dynamic/acoustic components or devices into the proposed general framework. A backing cavity can then be easily included into the current model. Detailed discussions about the modeling of a membrane-cavity coupling system can be found in our previous work.³⁸

III. NUMERICAL RESULTS AND ANALYSES

A. Mode classification inside the duct without flame

Before installing the heat source, natural modes inside the duct with periodic membranes, as well as their relationship with bandgaps, are first investigated and classified. This

is done by taking the flame interaction coefficient $n=0$ in the model. As to be detailed later, the salient feature of each type of mode calls for specific control actions to achieve modal stability after the heat source is added.

The following physical parameters are used in the numerical simulation: duct length $L=1.8$ m, height $h=0.045$ m, reflection coefficients $R_0=1$ (rigid boundary), $R_L=-1$ (pressure release boundary), sound speed in the air $c=345$ m/s, constant temperature 297 K, and air density $\rho_0=1.2$ kg/m³. Consider a duct comprising five unit-cells with a periodic distance $D=0.31$ m; the membrane parameters are taken as dimensionless tension $F^*=F/\rho_0c^2l=0.1$, dimensionless mass density $m^*=\rho_m/\rho_0l=1$, length $l=0.1$ m, and the first membrane position coordinate $x_1=0.1$ m, $x_2=0.2$ m. Considering a monopole sound source located in the left-hand portion of the duct $x_f=0.05$ m, the calculated transmitted sound pressure at the outlet is depicted in Fig. 2. Obvious low sound pressure bands can be obtained when considering the membranes. Exact Bloch wave theory, which is usually adopted for dispersion analyses in an infinite structure, is not used in here, since the number of cells is limited to five. Thus, the frequency regions, corresponding to low transmitted sound pressure, are loosely referred to as bandgaps here. A referenced threshold value as marked in Fig. 2(a) is used to determine the bandgap width, and the gray area gives an approximate range of the bandgap.

Obviously, the duct with five membrane-cells enables two types of bandgaps, namely the RBG and BBG, as evidenced by the representative acoustic wave distributions, shown in Fig. 2(b). Out of these bandgaps, at 200 Hz, sound propagates as a plane wave and slightly varies along the duct length. At 400 Hz within the BBG region, however, sound propagates as a plane wave, while decreasing rapidly downstream along the cells/duct. At 650 Hz in the RBG region, local resonance effects are evidenced by basically the same resonance behavior of the membrane-cells.

Eigenfrequencies of the duct-membrane system are depicted in Fig. 3(a), in which red blocks are the results

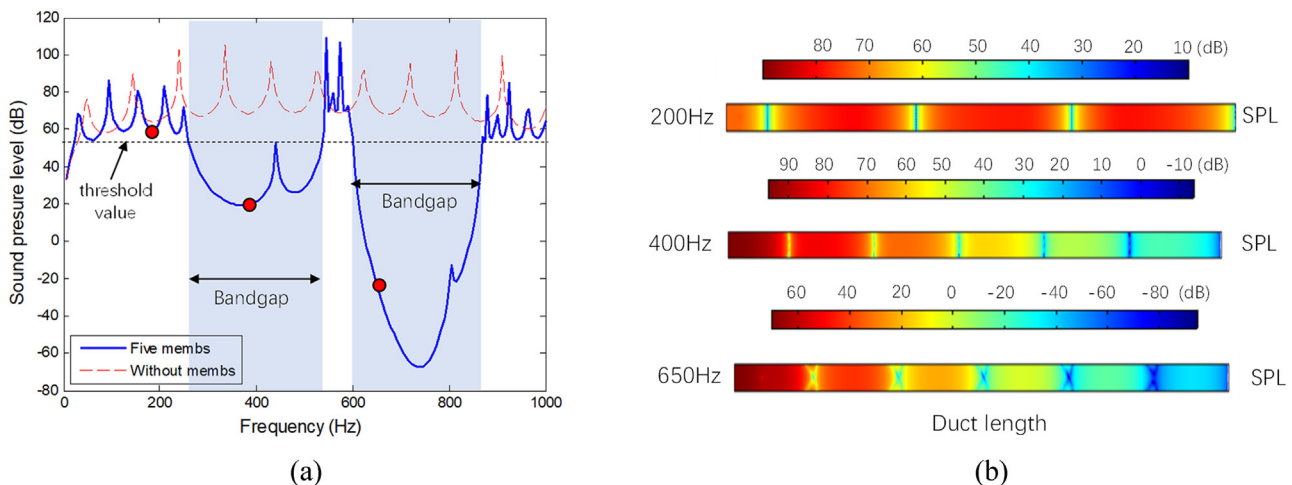


FIG. 2. (Color online) Bandgap characteristics for the duct embedded with five cells with no flame. (a) Sound pressure level; (b) sound pressure distributions.

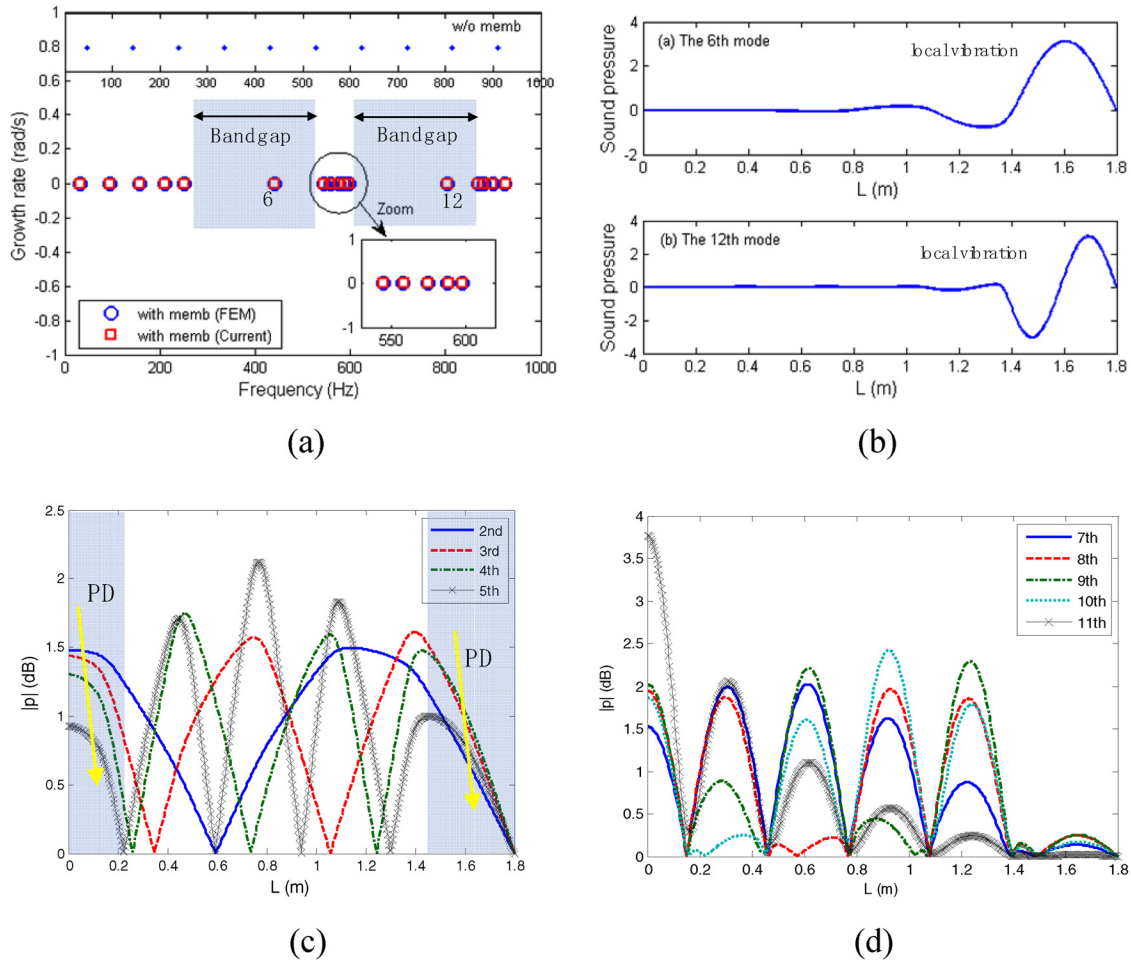


FIG. 3. (Color online) Modal characteristic description of the duct-periodic membranes system: (a) eigenfrequency distribution; (b) local mode shapes; (c) low-order mode shapes; (d) DMC mode shapes.

predicted by the current model alongside the FEA results marked by blue circles. For the latter, COMSOL Multiphysics[®] is used, in which Pressure Acoustics and Truss modular are used to simulate the sound field and the one-dimensional (1D) membrane structure, respectively. Normal Acceleration and Edge Load are applied to describe the coupling between the membrane and sound field inside the duct. In Fig. 3(a), the marked gray regions correspond to the bandgaps, and the natural frequencies of the duct (without membranes) are also given in this figure for easy comparison.

It can be seen that eigenfrequencies can be segmented into several groups due to the emergence of the bandgaps. The modes before the first bandgap are categorized as the so-called low-order modes; those few sparsely located inside the bandgaps can be referred to as local modes. Meanwhile, a region between the two bandgaps is noticed, which contains a cluster of densely populated modes. For convenience, this group of modes is called the dense modal cluster (DMC). Then the rest of the modes above the bandgap are considered as the high-order modes.

Figures 3(b)–3(d) show the mode shapes corresponding to the three types of modes: local, low-order, and DMC

modes, respectively. Obviously, the 6th and 12th modes belong to the local ones, for which high sound pressure region is delimited to a portion of the duct, namely, near the duct outlet in this case. Since the thermoacoustic characteristics depend on the sound pressure distribution or particle vibrational velocity as shown in Eq. (25), the system is most likely stable for these modes as the flame is placed in the minima region ($p \approx 0$) of sound pressure. Thus, the local modes remain stable in most circumstances (to be verified later).

Based on our previous study,⁷ it was found that the instabilities of thermoacoustic modes are determined by the relationship between the flame position and the acoustic mode shape. More specifically, the system is stable when the flame is located at the pressure drop (PD) region, but unstable at the pressure rise (PR) part, which is consistent with the well-known Rayleigh criterion. According to the above conclusion, these modes in different groups call for the specific control actions in relation with the flame position. Therefore, the low-order modes will be simultaneously stable when the flame is installed near the inlet and outlet of the duct, as marked in Fig. 3(c). Moreover, it is envisaged that these modes will be altered altogether by adjusting the

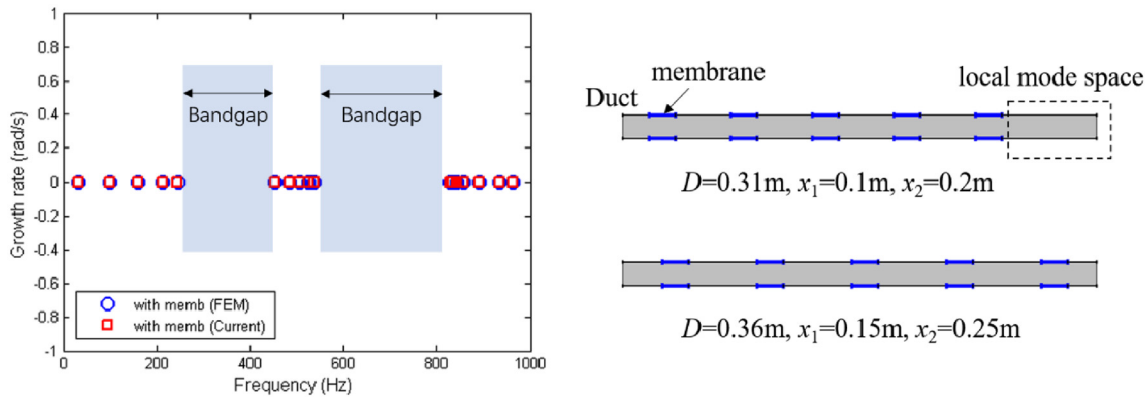


FIG. 4. (Color online) Modal characteristic description of the duct-periodic membrane system with different parameters, $D = 0.36\text{ m}$, $x_1 = 0.15\text{ m}$, and $x_2 = 0.25\text{ m}$.

bandgaps, which can be exploited for multi-modal instability suppression. This will be confirmed in Sec. III C.

Figure 3(d) shows that the DMC modes share varied yet similar spatial distributions except for the amplitudes (to better visualize the differences, no attempts were made to normalize the amplitudes). The similarity (and the tiny differences) among them is due to the vibration behavior of each membrane-cell, which is identical but installed at different locations. Based on the aforementioned PD-PR criterion,⁷ it is anticipated that these DMC modes would feature similar stability properties. It should be noted that the high-order mode characteristics are of less concern in practice. Therefore, no particular effort is paid to them in the subsequent analysis, although brief comments will be made in the instability analysis in Sec. III B.

Local modes can be avoided in the frequency band of interest through the adjustment of membrane position or the lattice length. For example, taking $D = 0.36\text{ m}$, $x_1 = 0.15\text{ m}$, and $x_2 = 0.25\text{ m}$, and keeping other parameters unchanged, the corresponding eigenfrequencies are plotted in Fig. 4. It follows that the local modes disappear in the entire frequency range up to 1000 Hz. The corresponding membrane distributions are also given in this figure; obviously, as $D = 0.36\text{ m}$, the membranes occupy the whole duct, limiting the space for accommodating the local modes.

B. Modal TAI control

This section discusses ways to control modal TAI of specific mode. To elucidate the instability control mechanism using bandgaps, a linear n - τ flame model is considered with the interaction coefficient $n = 0.5$, delay time $\tau = 0.2\text{ ms}$. These values fall into the common levels that were used in the literature,^{39,40} which are also conformable to the level of a practical combustion system. Different n and τ will naturally alter the modal characteristics of the system, which necessarily requires further adjustment of the bandgaps accordingly. Nevertheless, the basic bandgap-based control mechanism still holds. In addition, the flame located position is $x_q = 0.2\text{ m}$, and taking the same set of model parameters as Fig. 2, the first membrane position is

changed to $x_1 = 0.2\text{ m}$ and $x_2 = 0.3\text{ m}$. The modal characteristics of the thermo-vibro-acoustic coupling system, in terms of GR and frequency distribution, are displayed in Fig. 5, in which the red squares denote the system eigenfrequencies in the presence of periodic membranes, and the green circles correspond to the results without the membranes. As before, the bandgaps are marked by gray blocks.

An obvious stable local mode can be observed inside the first bandgap. For the current configuration, all modes remain stable in the frequency band 0–1000 Hz upon installing the membranes, rendering it possible to achieve multi-modal instability control capability. Similarly, these thermoacoustic modes are classified into several groups as presented in Sec. III A: the low-order, local, DMC, and high-order groups. Since there are few modes in the bandgaps, one can design the bandgap position based on the frequency band of interest, in which the instable modes can be avoided completely.

More specifically, low-order modal characteristics are studied in Fig. 6. Figure 6(a) shows the mode shapes, and Fig. 6(b) shows the corresponding complex eigenfrequencies (with GR). Three flame positions ($x_q = 0.2\text{ m}$, 0.45 m , and 0.7 m) are considered as marked by the vertical dashed lines, respectively. It can be found that the modal instabilities of this group of modes are closely related to the pressure state scenario of the flame position, in agreement with

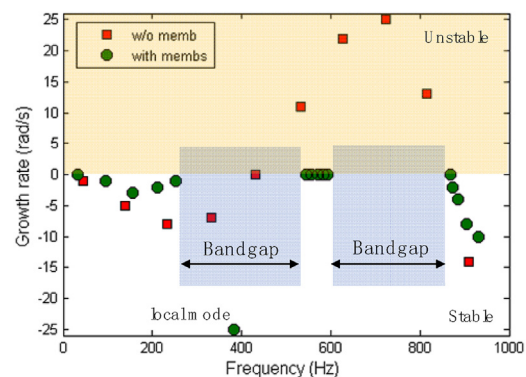


FIG. 5. (Color online) Modal instability suppression using five cells periodically arranged in the duct.

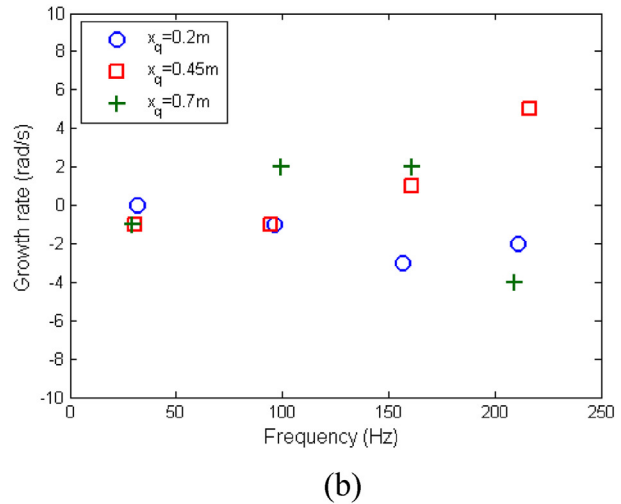
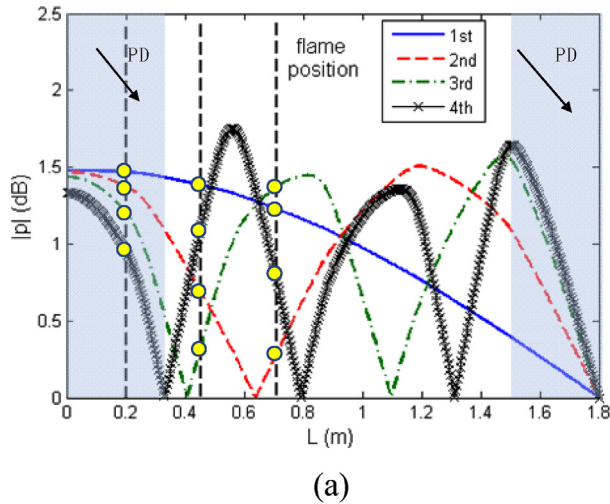


FIG. 6. (Color online) Mode shapes and their GRs for the modes in low frequency range. (a) Mode shape distribution; (b) eigenvalues for different flame positions.

the PD-PR criterion.⁷ More precisely, the system is stable when the flame is located at the PD region but unstable at the PR part. Based on this criterion, the first four modes are always stable when the flame is applied in the duct inlet or outlet region as marked by gray blocks in Fig. 6(a).

Figure 7(a) shows the mode shapes of the DMC, which regroups modes featuring similar mode shapes. Based on the PD-PR criterion, these DMC modes exhibit the same stability properties as presented in Fig. 7(b) for different flame positions ($x_q = 0.2\text{ m}$, 0.35 m , and 0.75 m); thus, proper adjustment of the flame position is essential for the stability of these DMC modes. Knowing the difficulty in adjusting the flame position once the system is built, the practical significance of the present study is rather to offer useful guidance at the design stage of the combustion chamber.

Figure 8 shows the mode shapes of the high-order mode group, exhibiting rather complex and irregular distributions. For this group of modes, however, their instability, whenever it occurs, is relatively easy to control through introducing reasonable damping in the system. Due to limitations of article length, their instable characteristics are not shown in

this paper, while the corresponding identically stable regions are marked by gray blocks in this figure, which are also in agreement with the PD-PR criterion.

The complex eigenvalues below 1000 Hz are given in Fig. 9 for three flame positions: $x_q = 0.2\text{ m}$, 0.45 m , and 0.75 m . It can be observed that the DMC modes and the local mode groups remain stable, whilst the low- and high-order modes may become unstable if the flame is inappropriately positioned. In this case, the adjustment of the flame position turns out to be an effective way to avoid the TAI since it is closely related to the pressure state scenario of the flame position. If the flame position cannot be changed for whatever practical reasons, a proper tuning of the parameters relating to the periodic membrane system should be considered. Possible system parameters include the lattice length, membrane tension, and other adjustable parameters in the system.

In a technical combustion system, high temperature is always present. Then materials with high temperature resistant coating for the membrane might be a possible way to achieve the functionality required in a high temperature environment. To alleviate the possible adverse added

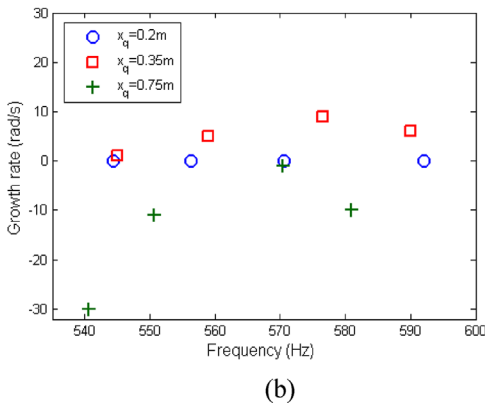
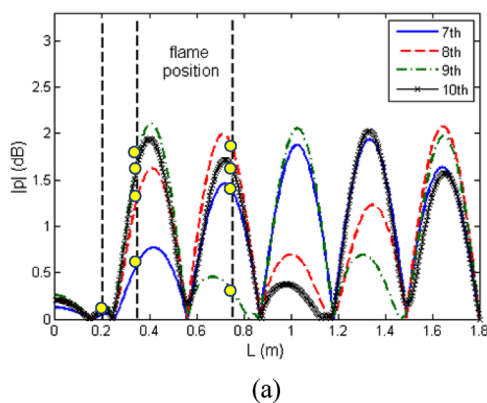


FIG. 7. (Color online) Mode shapes and their GRs for the characteristic modes in DMC area. (a) Mode shapes; (b) GRs.

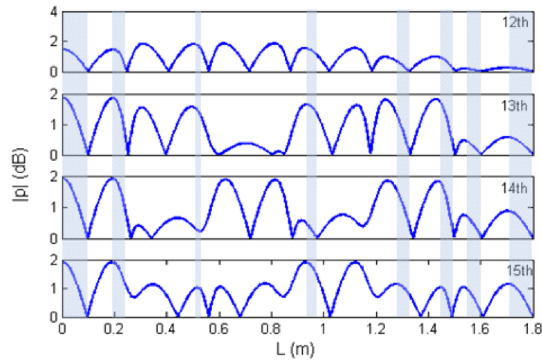


FIG. 8. (Color online) Mode shapes for the modes in high frequency range (the gray boxes indicate a stable state).

stiffness effects of the resistant coating, parameter tuning or optimization might be needed, which could be conducted under the present analysis framework. Meanwhile, we are also hopeful that advances in material science, heat treatment technology, and manufacturing capability would offer new possibilities, although nonexistent right now, to implement the idea developed in this paper.

C. Multi-modal instability control via resonant and Bragg bandgaps

Capitalizing on the aforementioned bandgap phenomena and their relationship with individual mode, we discuss ways to achieve simultaneous and multi-modal TAI control in this section. It is well known that the local RBGs are controlled by the stiffness and mass property of the unit-cells, while the BBGs mainly depend on the spatial impedance discontinuity among unit-cells and the lattice distance. Therefore, the effects of membrane tension F^* and lattice length D on the resonant and Bragg bandgaps are first studied in this section in the absence of flame (by setting $n = 0$).

The same set of parameters used in Fig. 5 is taken here. Corresponding results are presented in Fig. 10. Figure 10(a) shows the evolution of the BBG and RBG with different membrane tensions. Starting from the nominal case with

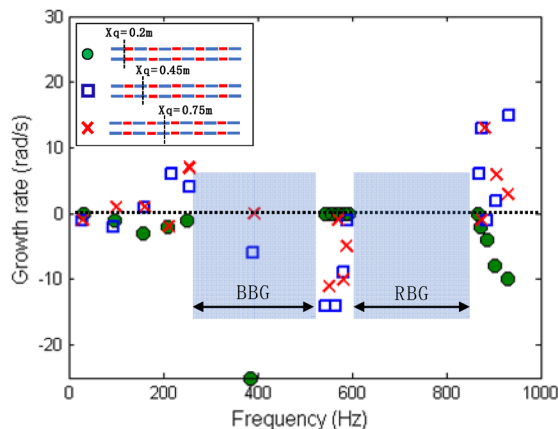


FIG. 9. (Color online) Instability control effect of periodical membranes for different flame positions, $x_q = 0.2$ m, 0.45 m, and 0.75 m.

$F^* = 0.06$ [middle part of Fig. 10(a)], three bandgaps can be clearly seen: one RBG in the middle of two adjacent BBGs. Through changing the tension of the membranes, the RBG is shifted and merged with the adjacent BBG to form a so-called coupled bandgap (CBG). Similarly, the same merging phenomenon can also be achieved through changing the lattice distance, as evidenced by Fig. 10(b).

With the aim to further study the evolutionary trend of BBG and RBG, their contours with respect to continuously varying membrane tension and periodic distance are produced and given in Fig. 11. As the membrane tension F^* increases, the RBG shifts to higher frequency, while the BBG shows little effect. Increasing the periodic distance D lowers the BBG frequency with negligible effects on the RBG. What is more, it can be seen that the RBG shows more effect on the sound field. Therefore, the RBGs can be easily tuned to change the ultimate bandgap features inside the duct. It is expected that such a tuning would impact the acoustic field inside the duct and the targeted control process.

To further substantiate this point, the influences of lattice distance and membrane tension on the modal instability control are displayed in Fig. 12. Taking the same flame and duct-membrane parameters as those used in Fig. 5, but two different lattice lengths $D = 0.21$ m and 0.11 m, the corresponding complex eigenfrequencies of the system are plotted in Figs. 12(a) and 12(b), respectively. Obviously, when the lattice distance decreases, the BBG is shifted to higher frequency, while these modes remain stable. Figures 12(c) and 12(d) give the distributions of complex eigenfrequencies when using a lower membrane tension $F^* = 0.05$. Instable modes can be found as the membrane tension decreases, which further suggests that the RBG (controlled by the membrane parameters) has a significant influence on the modal instability suppression. In other words, the parameters of the local membranes seem to be more important than the lattice length in terms of modal TAI control. Considering the nature of the RBG, it can be surmised that a strict periodicity is not essential, a point to be discussed and confirmed below.

To further consolidate the point in terms of the dominant role played by the RBG, another numerical example is given with $D = 0.21$ m, $x_1 = 0.5$ m, $x_2 = 0.6$ m, $x_q = 0.45$ m, $n = 0.5$, and $\tau = 0.2$ ms. The corresponding complex eigenfrequencies of the thermoacoustic system without the membranes are first plotted in Fig. 13(a), showing four instable modes in regions of 200–400 and 600–800 Hz. To stabilize these modes, two RBGs are constructed via using different membrane tensions, $F^* = 0.03$ and 0.12 , as shown in Figs. 13(b) and 13(c), respectively. It follows that obvious control effect is achieved as the RBG is formed near the instable modes.

Therefore, the modal instabilities can be effectively controlled by properly setting RBGs, although the eigenfrequency distributions are affected by both the RBG and BBG. This also means that the local or dense cluster regrouping modes can be avoided upon properly choosing

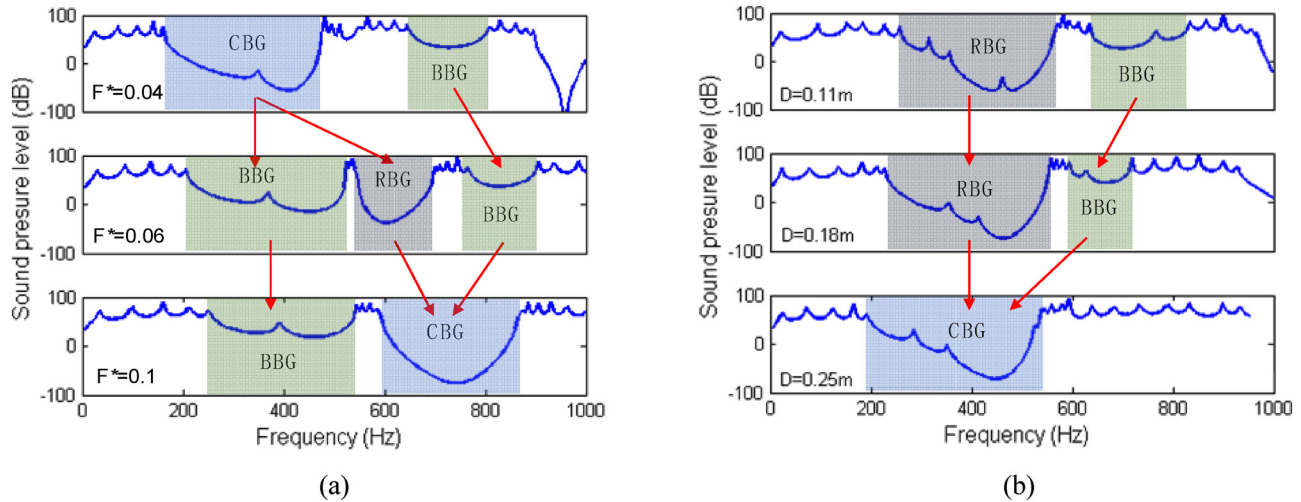


FIG. 10. (Color online) Evolutions of RBG and BBG with respect to membrane tension and lattice distance. (a) Varying the membrane tension; (b) varying the lattice distance.

appropriate membrane tension and lattice length as presented in Fig. 12. In practice, the tailoring of the RBGs should primarily be considered, along with a less stringent design of the BBGs.

Based on the above analyses, global and multi-modal control of TAI can be achieved. This can be materialized through the proper tuning of various parameters relating to the periodic structures under the practical constraints. The room for the tuning, however, is vast. For example, for multi-modal TAI control, the combination of different periodic structures can be considered. Should a specific frequency band be the control target, bandgap tuning and positioning should be an effective method to consider.

For a thermoacoustic system with periodically arranged local resonators, system optimizations can be considered to accommodate a given scenario and enhance the control performance. The bandgap position and its width can be taken as the optimization target for different combustion systems. The process naturally involves many system parameters,

exemplified by the membrane length and tension, lattice length, and spatial parameters relating to the installation locations. Existing optimization techniques provide abundant choices to carry out the optimization, such as the Bayesian optimization algorithm or the genetic algorithm.

Strict periodicity in periodic structures is difficult to achieve in practice, considering the installation and machining inaccuracy. This would lead to a quasi-periodical structure. To examine the issue and its influence on the control efficacy, we consider a few membranes having slightly different tensions F^* or the lattice lengths D . In the simulation model, a 10% deviation is introduced to the last two membrane-cells as $F' = F^* \times (1 + 10\%)$ and $D' = D \times (1 + 10\%)$. The deviation is from the nominal case studied in Fig. 13(b). Results of modal GR are shown in Fig. 14. It can be seen that a slight 10% deviation of D or F^* affects little the modal stabilities, especially for the low-order modes, demonstrating the robustness of the proposed control technique.

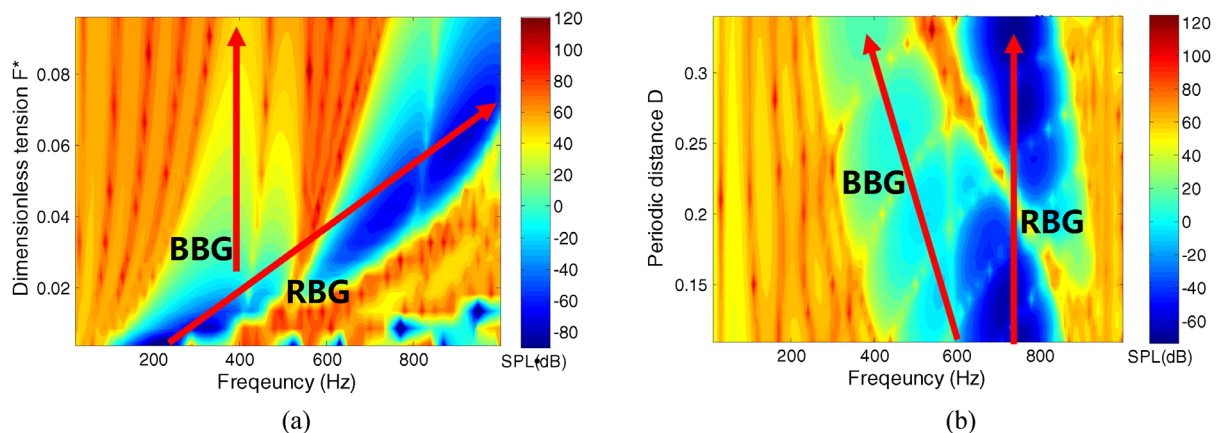


FIG. 11. (Color online) Contours of BBG and RBG with respect to continuously varying membrane tension and periodic distance. (a) $D = 0.31\text{ m}$ with varying membrane tension; (b) $F^* = 0.1$ with varying periodic distance.

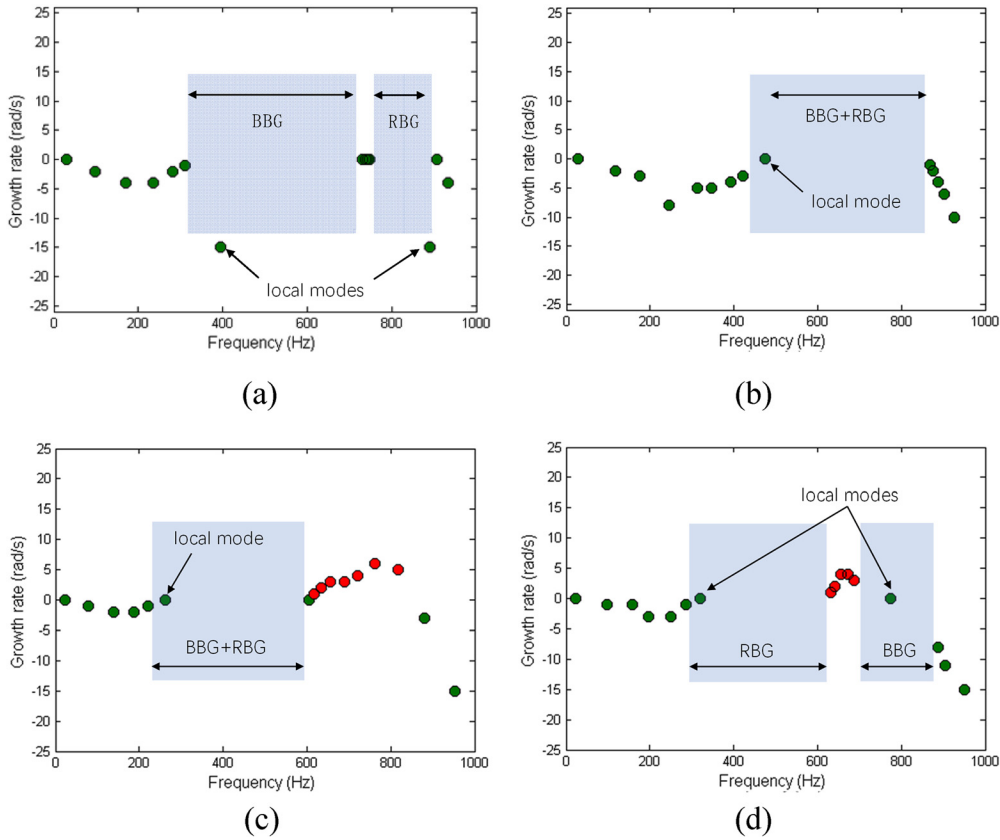


FIG. 12. (Color online) Modal instability analysis as taking different lattice length and membrane tension for the periodic system. (a) $D = 0.21$ m, $F^* = 0.1$; (b) $D = 0.11$ m, $F^* = 0.1$; (c) $D = 0.21$ m, $F^* = 0.05$; (d) $D = 0.11$ m, $F^* = 0.05$.

IV. CONCLUSIONS

In this paper, thermoacoustic oscillation in a heated duct is investigated, in which periodic and flush-mounted membrane-cells are proposed to control the modal TAI. An energy-based formulation in conjunction with a linear heat release $n-\tau$ model is established to model the thermo-vibroacoustic interaction among the duct acoustics, the membranes, and the heat source. The proposed model provides a novel and effective tool for the study and design of multiple thermoacoustic modal instability control systems.

The installation of periodically arranged membranes in the sidewalls of the duct entails two types of bandgaps, namely RBG and BBG. In relation to these bandgaps, vibroacoustic modes inside the duct can be categorized into several groups, referred to as low-order, local, DMC, and high-order modes. Different types of modes exhibit different modal features, thus, calling for different control strategies.

Significant modal instability suppression is obtained upon installing the periodic membranes into the duct system. The modal instabilities are shown to be closely related to the sound pressure status at the flame position, in agreement with the PD-PR criterion developed in our previous study. The first group of low-order modes are stable when

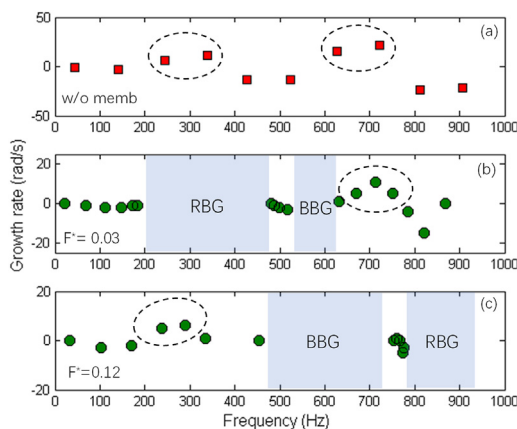


FIG. 13. (Color online) Modal instability control effects using different membrane tensions.

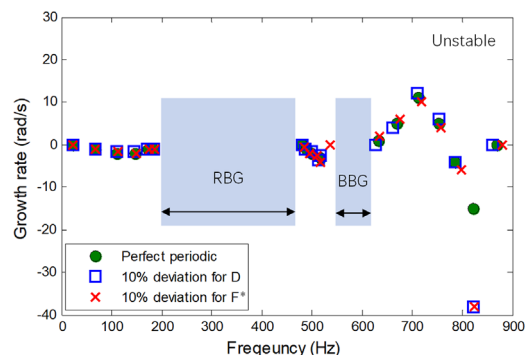


FIG. 14. (Color online) Modal instability control effects with D and F^* deviated by 10% from their nominal values used in Fig. 12(b).

the flame position approaches either the duct inlet or outlet. DMC modes share the same stability properties due to their close resemblance in terms of mode shapes. Through proper design and positioning of the membrane-induced bandgaps in accordance with the frequency band of interest, instable modes can be completely avoided.

To achieve effective and multi-modal TAI control, system parameters including membrane tension and lattice distance can be tuned. RBGs are shown to play a vital role in determining the sound pressure distribution inside the duct and, consequently, the TAI control performance as compared with the BBGs. Significant control effect can be achieved when the RBG is formed near the instable modes. Meanwhile, the proposed control method proves to be robust to a certain extent, since small deviations of the membrane tension or lattice distance can be tolerated. This is definitely conducive to practical implementation of the proposed control technique.

ACKNOWLEDGMENTS

This work is supported by the Research Grant Council of the Hong Kong SAR (Grant No. PolyU 152036/18E) and the National Natural Science Foundation of China (Grant Nos. 11972125 and 12102101).

¹F. E. C. Culick and V. Yang, "Prediction of the stability of the unsteady motions in solid propellant rocket motors," in *Nonsteady Burning and Combustion Stability of Solid Propellants* (AIAA, Reston, VA, 1992), Chap. 18, pp. 719–779.

²T. Lieuwen, H. Torres, C. Johnson, and B. T. Zinn, "A mechanism of combustion instability in lean premixed gas turbine combustors," *J. Eng. Gas Turb. Power* **123**, 182–189 (2001).

³S. Hubbard and A. P. Dowling, "Acoustic resonances of an industrial gas turbine combustion system," *J. Eng. Gas Turb. Power* **123**, 766–773 (2001).

⁴R. Gaudron and A. S. Morgan, "Thermoacoustic stability prediction using classification algorithms," *Data-Centric Eng.* **3**, E17–1–E17–16 (2022).

⁵A. P. Dowling and S. R. Stow, "Acoustic analysis of gas turbine combustors," *J. Propul. Power* **19**, 751–764 (2003).

⁶X. Xing, Q. Xu, J. T. Du, L. Cheng, and Z. G. Liu, "A modified Fourier series solution for a thermo-acoustic tube with arbitrary impedance boundaries," *Int. J. Appl. Mech.* **12**(5), 2050047 (2020).

⁷Y. Liu, J. T. Du, and L. Cheng, "Thermoacoustic modal instability and its suppression with locally resonant flexible membranes," *Combust. Flame* **237**, 111859 (2022).

⁸M. Hoeijmakers, V. Kornilov, I. L. Arteaga, P. de Goey, and H. Nijmeijer, "Intrinsic instability of flame-acoustic coupling," *Combust. Flame* **161**(11), 2860–2867 (2014).

⁹T. Emmert, S. Bomberg, and W. Polifke, "Intrinsic thermoacoustic instability of premixed flames," *Combust. Flame* **162**(1), 75–85 (2015).

¹⁰N. K. Mukherjee and V. Shriram, "Intrinsic flame instabilities in combustors: Analytic description of a 1D resonator model," *Combust. Flame* **185**, 188–209 (2017).

¹¹P. Barooah, T. J. Anderson, and J. M. Cohen, "Active combustion instability control with spinning valve actuator," *J. Eng. Gas Turbines Power* **125**(4), 925–932 (2003).

¹²A. Ghani and W. Polifke, "Control of intrinsic thermoacoustic instabilities using hydrogen fuel," *Proc. Combust. Inst.* **38**, 6077–6084 (2021).

¹³M. A. Heckl, "Active control from the noise of a Rijke tube," *J. Sound Vib.* **124**, 117–133 (1988).

¹⁴J. Hathout, A. M. Annaswamy, M. Fleifil, and A. F. Ghonlem, "Active control of thermoacoustic instability using a model-based approach," *Heat Transfer* **2**, 159–167 (1997).

¹⁵A. P. Dowling and A. S. Morgans, "Feedback Control of Combustion Oscillations," *Annu. Rev. Fluid Mech.* **37**(1), 151–182 (2005).

¹⁶U. Zalluhoglu and N. Olgac, "Deployment of time-delayed integral control for suppressing thermoacoustic instabilities," *J. Guid. Control Dyn.* **39**(10), 2284–2296 (2016).

¹⁷M. X. Zhang, J. X. Li, W. W. Cheng, and T. Li, "Active control of thermoacoustic instability using microsecond plasma discharge," *J. Appl. Phys.* **127**, 033301 (2020).

¹⁸N. Noiray and B. Schuermans, "Theoretical and experimental investigations on damper performance for suppression of thermoacoustic oscillations," *J. Sound Vib.* **331**(12), 2753–2763 (2012).

¹⁹D. Zhao and A. S. Morgans, "Tuned passive control of combustion instabilities using multiple Helmholtz resonators," *J. Sound Vib.* **320**(4), 744–757 (2009).

²⁰V. Bellucci, P. Flohr, C. O. Paschereit, and F. Magni, "On the use of Helmholtz resonators for damping acoustic pulsations in industrial gas turbines," *J. Eng. Gas Turb. Power* **126**(2), 271–275 (2004).

²¹I. D. J. Dupere and A. P. Dowling, "The use of Helmholtz resonators in a practical combustor," *J. Eng. Gas Turb. Power* **127**(2), 268–275 (2005).

²²U. Zalluhoglu and N. Olgac, "A study of Helmholtz resonators to stabilize thermo-acoustically driven pressure oscillations," *J. Acoust. Soc. Am.* **139**, 1962–1973 (2016).

²³Z. G. Zhang, D. Zhao, N. M. Han, S. H. Wang, and J. W. Li, "Control of combustion instability with a tunable Helmholtz resonator," *Aerosp. Sci. Technol.* **41**, 55–62 (2015).

²⁴R. Corá, C. A. Martins, and P. T. Lacava, "Acoustic instabilities control using Helmholtz resonators," *Appl. Acoust.* **77**, 1–10 (2014).

²⁵L. Li, Z. H. Guo, C. Y. Zhang, and X. F. Sun, "A passive method to control combustion instabilities with perforated liner," *Chin. J. Aeronaut.* **23**(6), 623–630 (2010).

²⁶U. Zalluhoglu and N. Olgac, "Passive suppression of thermoacoustic instability in a Rijke tube," *IFAC-Papers OnLine* **49**(10), 59–64 (2016).

²⁷D. Zhao, E. Gutmark, and A. Reinecke, "Mitigating self-excited flame pulsating and thermoacoustic oscillations using perforated liners," *Sci. Bull.* **64**(13), 941–952 (2019).

²⁸G. Y. Zhang, X. Y. Wang, L. Li, X. D. Jing, and X. F. Sun, "Control of thermoacoustic instability with a drum-like silencer," *J. Sound Vib.* **406**, 253–276 (2017).

²⁹M. Sigalas and E. N. Economou, "Band structure of elastic waves in two dimensional systems," *Solid State Commun.* **86**, 141–143 (1993).

³⁰M. Sigalas, "Defect states of acoustic waves in a two-dimensional lattice of solid cylinders," *J. Appl. Phys.* **84**, 3026–3030 (1998).

³¹Z. Liu, X. Zhang, Y. Mao, Y. Y. Zhu, Z. Y. Yang, C. T. Chan, and P. Sheng, "Locally resonant sonic materials," *Science* **289**, 1734–1736 (2000).

³²Y. F. Li, H. J. Shen, L. K. Zhang, Y. S. Su, and D. L. Yu, "Control of low-frequency noise for piping systems via the design of coupled band gap of acoustic metamaterials," *Phys. Lett. A* **380**, 2322–2328 (2016).

³³X. Wang and C. M. Mak, "Wave propagation in a duct with a periodic Helmholtz resonators array," *J. Acoust. Soc. Am.* **131**, 1172–1182 (2012).

³⁴X. N. Wang, W. Y. Zhu, and Y. D. Zhou, "Sound transmission in a duct with a side-branch tube array mounted periodically," *J. Acoust. Soc. Am.* **139**, EL202–EL208 (2016).

³⁵X. F. Shi and C. M. Mak, "Sound attenuation of a periodic array of micro-perforated tube mufflers," *Appl. Acoust.* **115**, 15–22 (2017).

³⁶Y. Liu, J. T. Du, and L. Cheng, "Bandgap formation under temperature-induced quasi-periodicity in an acoustic duct with flexible walls," *J. Sound Vib.* **486**, 115615 (2020).

³⁷Y. Liu and J. T. Du, "Sound attenuation analysis and optimal design for a duct with periodic membranes embedded in its sidewalls," *J. Appl. Phys.* **125**, 034901 (2019).

³⁸Y. Liu and J. T. Du, "Coupling effects of boundary restraining stiffness and tension force on sound attenuation of a cavity-backed membrane duct silencer," *Appl. Acoust.* **117**, 150–159 (2017).

³⁹F. Nicoud, L. Benoit, C. Sensiau, and T. Poinot, "Acoustic modes in combustors with complex impedances and multidimensional active flames," *AIAA J.* **45**(2), 426–441 (2007).

⁴⁰Y. Yang, X. Liu, and Z. Zhang, "Large eddy simulation calculated flame dynamics of one F-class gas turbine combustor," *Fuel* **261**, 116451 (2020).